Biomedicine & Pharmacotherapy 179 (2024) 117303

Contents lists available at ScienceDirect

Biomedicine & Pharmacotherapy

journal homepage: www.elsevier.com/locate/biopha

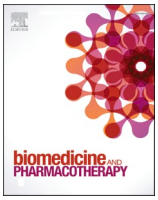

PPARβ/δ attenuates hepatic fibrosis by reducing SMAD3 phosphorylation and p300 levels via AMPK in hepatic stellate cells

Meijian Zhang [a,b,c,d], Emma Barroso [a,b,c,d,*], Lucía Peña [a,b,c,d], Patricia Rada [c,e], Ángela M. Valverde [c,e], Walter Wahli [f,g,h], Xavier Palomer [a,b,c,d], Manuel Vázquez-Carrera [a,b,c,d,*,1]

[a] Department of Pharmacology, Toxicology and Therapeutic Chemistry, Faculty of Pharmacy and Food Sciences, Spain
[b] Institute of Biomedicine of the University of Barcelona (IBUB), University of Barcelona, Barcelona 08028, Spain
[c] Spanish Biomedical Research Center in Diabetes and Associated Metabolic Diseases (CIBERDEM)-Instituto de Salud Carlos III, Madrid 28029, Spain
[d] Pediatric Research Institute-Hospital Sant Joan de Déu, Esplugues de Llobregat 08950, Spain
[e] Instituto de Investigaciones Biomédicas Sols-Morreale (CSIC/UAM), Madrid, Spain
[f] Center for Integrative Genomics, University of Lausanne, Lausanne CH-1015, Switzerland
[g] Lee Kong Chian School of Medicine, Nanyang Technological University, Singapore 308232, Singapore
[h] ToxAlim (Research Center in Food Toxicology), INRAE, UMR1331, Toulouse Cedex F-31300, France

ARTICLE INFO

Keywords:
PPARβ/δ
AMPK
ERK1/2
P300
Fibrosis
LX-2

ABSTRACT

The role of peroxisome proliferator-activated receptor (PPAR)β/δ in hepatic fibrosis remains a subject of debate. Here, we examined the effects of a PPARβ/δ agonist on the pathogenesis of liver fibrosis and the activation of hepatic stellate cells (HSCs), the main effector cells in liver fibrosis, in response to the pro-fibrotic stimulus transforming growth factor-β (TGF-β). The PPARβ/δ agonist GW501516 completely prevented glucose intolerance and peripheral insulin resistance, blocked the accumulation of collagen in the liver, and attenuated the expression of inflammatory and fibrogenic genes in mice fed a choline-deficient high-fat diet (CD-HFD). The antifibrogenic effect of GW501516 observed in the livers CD-HFD-fed mice could occur through an action on HSCs since primary HSCs isolated from *Ppard*$^{-/-}$ mice showed increased mRNA levels of the profibrotic gene *Col1a1*. Moreover, PPARβ/δ activation abrogated TGF-β1-mediated cell migration (an indicator of cell activation) in LX-2 cells (immortalized activated human HSCs). Likewise, GW501516 attenuated the phosphorylation of the main downstream intracellular protein target of TGF-β1, suppressor of mothers against decapentaplegic (SMAD)3, as well as the levels of the SMAD3 co-activator p300 via the activation of AMP-activated protein kinase (AMPK) and the subsequent inhibition of extracellular signal-regulated kinase-1/2 (ERK1/2) in LX-2 cells. Overall, these findings uncover a new mechanism by which the activation of AMPK by a PPARβ/δ agonist reduces TGF-β1-mediated activation of HSCs and fibrosis via the reduction of both SMAD3 phosphorylation and p300 levels.

1. Introduction

Liver fibrosis is a wound healing process characterized by the accumulation of extracellular matrix (ECM) proteins, mostly crosslinked type I and III collagens, which ultimately leads to impaired liver function [1]. It develops as a result of chronic inflammation and cell apoptosis in various diseases including viral hepatitis, alcohol-related liver disease (ALD), and metabolic dysfunction-associated steatotic liver disease (MASLD, formerly referred to as nonalcoholic fatty liver disease [NAFLD]). MASLD, which is considered a hepatic manifestation of insulin resistance, ranges from steatotic liver disease to metabolic dysfunction-associated steatohepatitis (MASH). The latter is characterized by hepatocyte ballooning, indicative of hepatocellular damage, and liver inflammation, with or without fibrosis. Remarkably, in patients with significant fibrosis, MASLD progresses more rapidly to cirrhosis or hepatocellular carcinoma [2].

The development and progression of liver fibrosis are under the control of a complex network of signaling pathways among many cell

* Correspondence to: Unitat de Farmacologia, Facultat de Farmàcia i Ciències de l'Alimentació, Av. Joan XXIII 27-31, Barcelona E-08028, Spain.
E-mail addresses: ebarroso@ub.edu (E. Barroso), mvazquezcarrera@ub.edu (M. Vázquez-Carrera).
[1] Lead contact.

https://doi.org/10.1016/j.biopha.2024.117303
Received 5 June 2024; Received in revised form 4 August 2024; Accepted 13 August 2024
Available online 18 August 2024
0753-3322/© 2024 The Author(s). Published by Elsevier Masson SAS. This is an open access article under the CC BY license (http://creativecommons.org/licenses/by/4.0/).

types. The activation of hepatic stellate cells (HSC) in response to chronic liver injury is a critical step in the pathogenesis of liver fibrosis [1,3]. In fact, activated HSCs have been reported to be the main producers of ECM during hepatic fibrogenesis [4,5]. In the healthy liver, HSCs reside in the perisinusoidal space in a quiescent state. However, after chronic liver injury, HSCs are activated by profibrotic stimuli and undergo transdifferentiation into proliferative, migratory, fibrogenic, myofibroblast-like cells [6], which show upregulated expression of α-smooth muscle actin (αSMA), a marker of the myofibroblast phenotype, and produce collagen I.

Transforming growth factor-β (TGF-β) is the best-studied pro-fibrotic stimulus. This pleiotropic cytokine is produced during disease progression by infiltrating lymphocytes and monocytes, tissue-resident macrophages, and damaged hepatocytes [7]. TGF-β is also produced by activated HSCs, thus leading to a feedforward loop that perpetuates fibrogenesis [8]. TGF-β signaling in HSCs induces the levels of αSMA, which gives myofibroblasts their contractility, enhances type I collagen production, and promotes HSC migration [1]. The TGF-β1 isoform, a major driver of human fibrotic pathologies [9], binds to its cell surface receptor complex and subsequently leads to the activation of kinase domains within the receptor complex, which potentiates phosphorylation cascades acting on transcriptional regulators of the suppressor of mothers against decapentaplegic (SMAD). Once activated by phosphorylation, SMADs translocate into the nucleus, where they bind to the SMAD binding element and drive the expression of key ECM genes, including those encoding collagens, fibronectin, and plasminogen activator inhibitor-1 (PAI-1) [10]. Interestingly, the transcriptional co-activator p300 cooperates with SMAD proteins to enhance the expression of their target genes, thereby playing a pivotal role in fibrotic responses [11]. TGF-β1 can also activate non-SMAD signaling pathways, such as the mitogen-activated protein kinase (MAPK) signaling cascade that includes extracellular signal-regulated kinase 1/2 (ERK1/2), which directly phosphorylates SMAD proteins, thus controlling their activity [12]. Of note, this positive crosstalk between TGF-β1 and ERK1/2 has been reported to contribute to HSC activation and liver fibrosis [13–15].

Peroxisome proliferator-activated receptors (PPARs) regulate several pathways involved in MASH pathogenesis [16]. Thus, agonists of these nuclear receptors could be potential therapeutic agents for the treatment of this disease. The PPARβ/δ isotype is expressed in the main liver cell types (hepatocytes, Kupffer cells, cholangiocytes, and HSCs) [17] and its activation hinders the progression of MASLD by ameliorating insulin resistance, reducing lipotoxicity, and alleviating inflammation and endoplasmic reticulum (ER) stress [16,18]. Several of these effects elicited by PPARβ/δ activation are mediated by the activation of AMP-activated protein kinase (AMPK), a central regulator of multiple metabolic pathways [19]. Interestingly, an inhibitory crosstalk between AMPK and ERK1/2 has been reported in myotubes [20], with the inhibition of ERK1/2 promoting AMPK activation and vice versa [21]. However, it is currently unknown whether this mechanism operates in HSCs. In addition, although PPARβ/δ has been proposed to play a role in liver fibrosis, the role of this nuclear receptor in HSC proliferation remains unclear [22], since some studies report that PPARβ/δ promotes HSC proliferation and fibrosis [23,24], whereas others suggest the opposite [17,25]. Therefore, further studies are needed to clarify the dual roles of PPARβ/δ in the pathogenesis of liver fibrosis.

Here, we show that PPARβ/δ activation improves liver steatosis in mice fed a choline-deficient high-fat diet (CD-HFD), a model of MASH that presents obesity and insulin resistance. In LX-2 cells, PPARβ/δ activation abrogates TGF-β1-induced HSC activation and SMAD3 phosphorylation via AMPK activation and the subsequent inhibition of the ERK1/2 pathway. These findings highlight ERK1/2 as a key target of AMPK and activated PPARβ/δ in the prevention of HSC activation and fibrosis.

2. Materials and methods

2.1. Reagents

GW501516, A769962, and U0126 were purchased from Sigma-Aldrich (Madrid, Spain), while TGF-β1 was obtained from R&D Systems (Minneapolis, MN, USA). Control and AMPKα1/2 siRNAs were purchased from Santa Cruz (Dallas, TX, USA).

2.2. In vivo studies

Male C57BL/6 mice (10–12 weeks old) (Envigo, Barcelona, Spain) were housed and maintained under a constant temperature (22 ± 2°C) and humidity (55 %). The mice had free access to water and food and were subjected to 12-h light-dark cycles. After 1 week of acclimatization, the mice were randomly distributed into three experimental groups (n = 6 each) and fed either standard chow (one group) or a choline-deficient high-fat diet (CD-HFD; 44.9 kcal% fat, 35.1 kcal% carbohydrates, and 20.0 kcal% protein, without added choline; D05010402, Research Diets, New Brunswick, NJ, USA) (two groups) for 12 weeks. The mice fed standard chow and one of the groups fed the CD-HFD received one daily p.o. gavage of vehicle (0.5 % w/v carboxymethylcellulose), while the remaining group fed the CD-HFD received one daily p.o. dose of 5 mg/kg/day of the PPARβ/δ agonist GW501516 dissolved in the vehicle (volume administered, 1 ml/kg) for 4 weeks. This dose of GW501516 has been reported to selectively activate PPARβ/δ, but not PPARα or PPARγ [26]. At the end of the treatment, the mice were sacrificed, and liver samples were frozen in liquid nitrogen before storage at −80ºC.

For the glucose tolerance test (GTT) and insulin tolerance test (ITT), the animals received 2 g/kg of body weight of glucose and 0.75 IU/kg of body weight of insulin, respectively, through an i.p. injection. Blood was collected from the tail at 0, 15, 30, 60, and 120 min.

HSCs were isolated by the collagenase-pronase perfusion of the livers of male (8–9 weeks old) *Ppard*-knockout (*Ppard*$^{-/-}$) mice (n = 6) and their wild-type littermates (*Ppard*$^{+/+}$) [27], as described originally by Friedman and Roll [28], using the minor modifications introduced by Rippe and co-workers [29]. Once isolated, the HSCs were immediately resuspended in TRIzol reagent (Sigma Aldrich, St. Louis, MO, USA) for RNA extraction.

All experiments were performed in accordance with the European Community Council directive 86/609/EEC. The experimental protocols as well as the number of animals used, determined based on the expected effect size, were approved by the Institutional Animal Care and Use Committee of the University of Barcelona. The reporting of the animal studies complied with the ARRIVE guidelines [30].

2.3. Liver histology

For histological staining studies, 4-μm thick sections obtained from formalin-fixed paraffin-embedded samples were stained with hematoxylin and eosin (H&E) to assess liver histology. Oil Red O (ORO) staining (Sigma-Aldrich) was conducted to assess lipid content. Sirius red and Masson's trichrome staining were conducted to assess fibrosis. Sirius red, Masson's trichrome, and ORO staining (Sigma-Aldrich) were performed on frozen 10-μm thick liver sections. Twelve images at a magnification of 20x were captured to quantify the red-stained collagen or lipid droplets, with the red-stained area evaluated per total area using ImageJ (National Institutes of Health, USA).

2.4. Cell culture

LX-2 cells (immortalized activated human HSCs) were kindly provided by Dr. Wladimiro Jiménez (Hospital Clínic de Barcelona). Cells were plated in 6-well plates at a density of 1.2×10^5 cells per well and grown to 70 %-80 % confluence. Cells were maintained in Dulbecco's

Modified Eagle's Medium (DMEM) containing 10 % fetal bovine serum (FBS; Hyclone, Logan, Utah, USA) and 50 units/ml of penicillin/streptomycin at 37 ºC in a humidified atmosphere with 5 % CO_2. LX-2 cells were pre-incubated in serum-free DMEM in the absence (control cells) or presence of GW501516 (10 μM), a concentration that selectively activates PPARβ/δ [31], or A769662 (60 μM) for 24 h and then exposed to vehicle or TGF-β1 (10 ng/ml) in the absence or presence of GW501516 or A769662 (60 μM) for an additional 24 h. LX-2 cells were also incubated in the absence (control cells) or presence of TGF-β1 (10 ng/ml) and co-incubated with U0126 (10 μM) for 24 h. All the cell experiments were repeated at least 3 times and there were 2 replicates in each experiment.

LX-2 cells were transiently transfected with 70 nM of siRNA against AMPKα1/2 (Santa Cruz Biotechnology Inc., catalogue sc-45312) or control siRNA (Santa Cruz Biotechnology Inc., catalogue sc-37007) in Opti-MEM medium (Thermo Fisher Scientific, MA, USA), using Lipofectamine 2000 (Invitrogen, Carlsbad, CA, USA) (13.2 μl per 2.2-ml well) according to the manufacturer's instructions. Compounds were tested after 24 h of transfection.

2.5. Wound healing assay

LX-2 cells were seeded at a concentration of 8×10^4 cells/well in a 12-well culture plate for 24 h. When the confluence reached > 90 %, cells were treated as mentioned and a cell-free are was made using a yellow tip. The cell monolayer was then washed twice with PBS. Microphotographs were taken on an inverted microscope immediately at the scratch (0 h) and endpoint of the experiment (24 h). The formula used for calculating the relative migration distance was as follows: relative migrating distance in % = [(D0-D24)/D0] x100.

2.6. Reverse transcription polymerase chain reaction and quantitative polymerase chain reaction

Isolated RNA was reverse transcribed to obtain 1 μg of complementary DNA (cDNA) using Random Hexamers (Thermo Fischer Scientific), the 10 mM deoxynucleotide (dNTP) mix, and the reverse transcriptase enzyme derived from the Moloney murine leukemia virus (MMLV, Thermo Fisher Scientific). The protocol was run in a thermocycler (BioRad) and consisted of a program with different steps and temperatures: 65°C for 5 min, 4°C for 5 min, 37°C for 2 min, 25°C for 10 min, 37°C for 50 min and 70°C for 15 min. The relative levels of specific mRNAs were assessed by real-time RT-PCR in a 96-well StepOnePlus Real-Time PCR System (Thermo Fisher Scientific) using the SYBR Green Master Mix (Applied Biosystems) and ROX, as previously described [23]. Briefly, samples contained a final volume of 20 μl, with 25 ng of total cDNA, 0.9 μM of the primer mix, and 10 μl of the mixture (the ratio of 2x SYBR Green Master Mix to ROX was 1000:1). The thermal cycler protocol for real-time PCR included the first step of denaturation at 95°C for 10 min followed by 40 repeated cycles of denaturation, primer annealing, and amplification at 95°C for 15 s, 60°C for 30 s, and 72°C for 30 s, respectively. Primer sequences were designed using the Primer-BLAST tool (NCBI), based on full mRNA sequences to find the optimal primers for amplification, and evaluated with the Oligo-Analyzer tool (Integrated DNA Technologies) to ensure optimal melting temperature (Tm) and avoid the formation of homo/heterodimers or nonspecific structures that can interfere with the interpretation of the results. The primer sequences were designed to specifically span the junction between exons and are provided in Supplementary Table 1. Values were normalized to expression levels of glyceraldehyde-3-phosphate dehydrogenase (*Gapdh*) or adenine phosphoribosyltransferase (*Aprt*), and measurements were performed in triplicate. All expression changes were normalized to the untreated control.

2.7. Immunoblotting

The isolation of total protein extracts was performed as described elsewhere [25]. Immunoblotting was performed with antibodies against α-SMA (#14–9760–82, Invitrogen, Carlsbad, CA, USA), AMPK (#2532, Cell Signaling Technology, Danvers, MA, USA), $pAMPK^{T172}$ (#2531, Cell Signaling Technology), GAPDH (MAB374, Millipore Sigma, Burlington, MA, USA), SMAD3 (#9513, Cell Signaling Technology), $pSMAD3^{S423/425}$ (#9520, Cell Signaling Technology), ERK1/2 (p44/42 MAPK) (#9194, Cell Signaling Technology), pERK1/2 (p44/42 MAPK) Thr^{202}/Tyr^{204} (#9101, Cell Signaling Technology), COL1A1 (#91144, Cell Signaling Technology), and p300 (#sc-585, Santa Cruz Biotechnology Inc., Dallas, TX, USA). Signal acquisition was performed using the Amersham™ Imager 600 apparatus and quantification of the immunoblot signal was performed with the Bio-Rad Image Lab software. The results for protein quantification were normalized to the levels of a control protein (GAPDH, α-tubulin or TBP) to avoid unwanted sources of variation.

2.8. Statistics

Results are expressed as the mean ± SEM. Significant differences were assessed by either Student's-t test or one-way and two-way ANOVA, according to the number of groups compared, using the GraphPad Prism program (version 10.2.0) (GraphPad Software Inc., San Diego, CA, USA). When significant variations were found by ANOVA, the Tukey-Kramer post-hoc test for multiple comparisons was performed only if F achieved a p-value < 0.05. Differences were considered significant at $p < 0.05$.

3. Results

3.1. PPARβ/δ activation improves hepatic fibrosis in mice fed the CD-HFD diet

First, we evaluated whether the PPARβ/δ agonist GW501516 ameliorated the metabolic alterations caused by the CD-HFD in mice. GW501516 did not reduce the increase in body weight caused by the CD-HFD (Fig. 1A), but it completely prevented the glucose intolerance (Fig. 1B). Mice fed the CD-HFD displayed an increase in peripheral insulin resistance that was not significant compared to the control mice, whereas GW50156 administration abolished the effect of the diet (Fig. 1C). H&E and ORO staining of liver sections showed that the CD-HFD caused significant hepatic lipid accumulation, which was reduced by GW501516 treatment (Fig. 1D-E). In addition, the CD-HFD resulted in a significant increase in the accumulation of collagen in the liver, as demonstrated by the Sirius red staining, whereas Masson's trichrome staining showed a non-significant increase (Fig. 1F-G). In both cases, GW501516 reduced collagen accumulation to values similar to those present in the control mice. Consistent with the histological findings, the CD-HFD increased the expression levels of hepatic fibrosis markers *Col1a1* and *Col3a1*, while GW501516 mitigated these increases, although the differences were not significant for the later (Fig. 2A). Moreover, although the CD-HFD increased the expression of the inflammatory genes *Ccl2* (also known as *Mcp1*) and *Tnfa,* GW501516 only significantly abrogated the expression of the former, with GW501516 also reducing the mRNA levels of *Il6* (Fig. 2B). GW501516 prevented the increase in the hepatic expression of *Tgfb* as well as that of the SMAD3-target gene *Ctgf*, whereas the expression of *Serpine1*, which encodes PAI-1, was not affected (Fig. 2C). M1 macrophages contribute to MASH progression by promoting the secretion of inflammatory cytokines, while M2 macrophages exert anti-inflammatory effects [32]. Interestingly, it has been reported that PPARβ/δ regulates macrophage polarization towards the anti-inflammatory M2 phenotype [33]. In agreement with this, GW501516 completely abolished the increase in the expression of the M1 marker *Nos2* caused by the CD-HFD, while preventing the

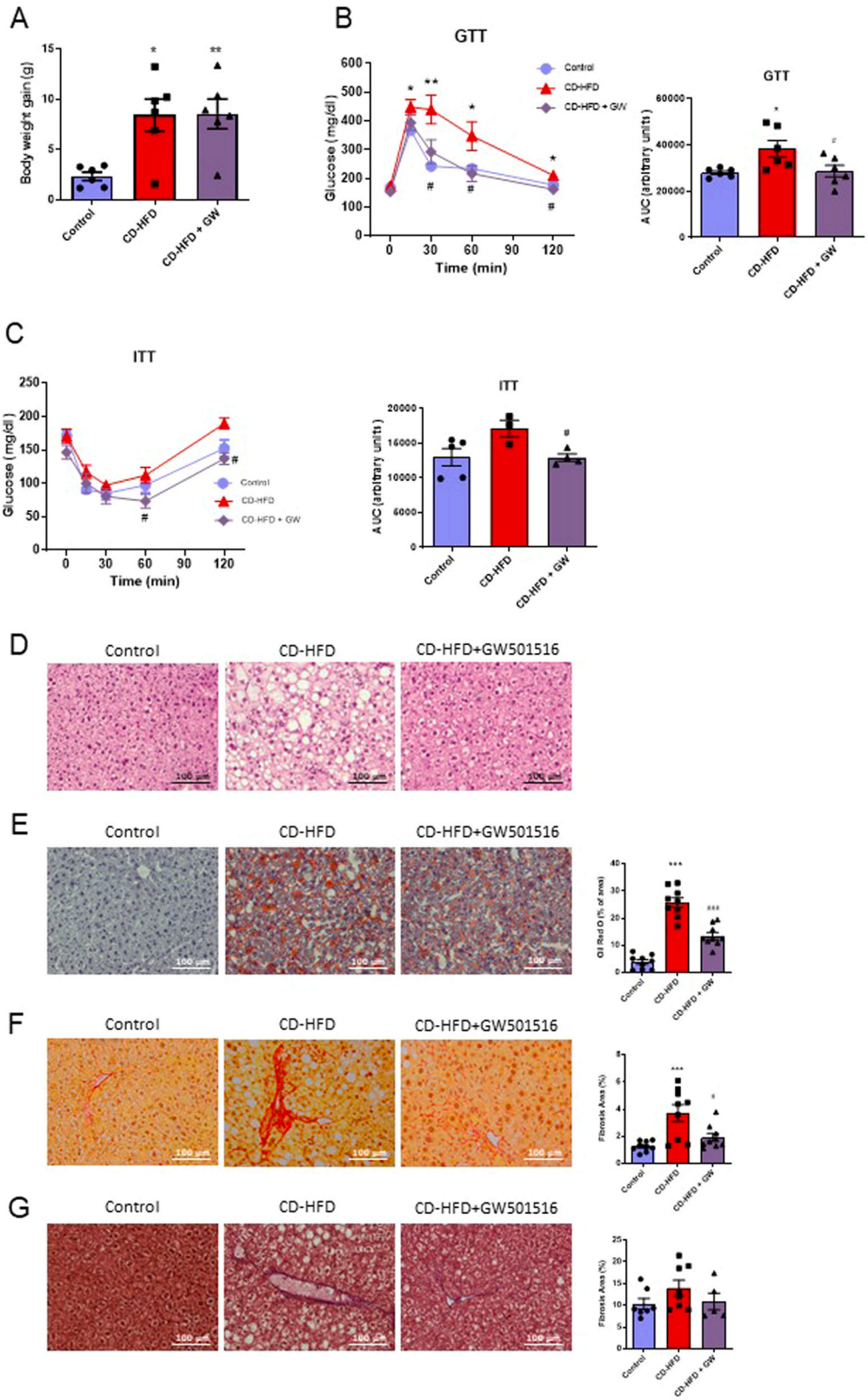

Fig. 1. PPARβ/δ activation improves hepatic fibrosis in mice fed a CD-HFD. (**A**) Body weight gain in control mice, mice fed the CD-HFD for 12 weeks, and mice fed the CD-HFD for 12 weeks and treated with the PPARβ/δ agonist GW501516 for the last 4 weeks (weeks 9–12). n = 6 per group. (**B**) GTT and area under the curve (AUC). n = 6 per group. (**C**) ITT and AUC. n = 6 per group. Representative images of liver sections and quantification of hematoxylin–eosin (H&E) (**D**), Oil Red O (ORO) (**E**), Sirius red (**F**), and Masson's trichrome (**G**) staining in control mice, mice fed the CD-HFD for 12 weeks, and mice fed the CD-HFD for 12 weeks and treated with the PPARβ/δ agonist GW501516 for the last 4 weeks. Scale bar: 100 μm. Data are presented as the mean ± SEM. Significant differences were established by ANOVA. ***$p < 0.001$, **$p < 0.01$, and *$p < 0.05$ *vs.* control. $^{###}p < 0.001$, $^{##}p < 0.01$, and $^{#}p < 0.05$ *vs.* mice fed the CD-HFD.

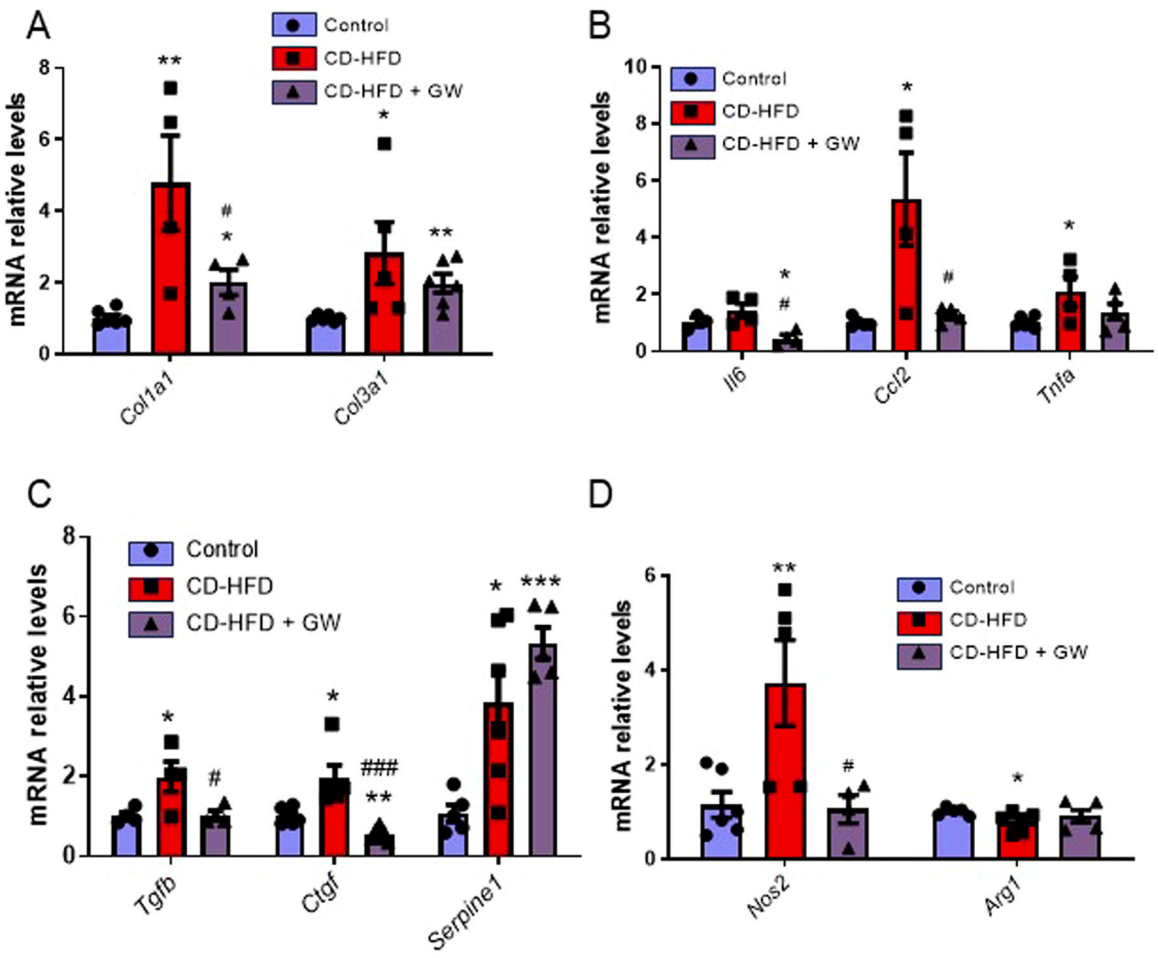

Fig. 2. PPARβ/δ activation regulates the hepatic mRNA levels of markers of fibrosis, inflammation and macrophage polarization in mice fed a CD-HFD. (**A**) mRNA levels of the fibrotic markers *Col1a1* and *Col3a1* in the livers of control mice, mice fed the CD-HFD for 12 weeks and mice fed the CD-HFD for 12 weeks and treated with the PPARβ/δ agonist GW501516 for the last 4 weeks (weeks 9–12). (**B**) mRNA levels of the inflammatory markers *Il6, Ccl2*, and *Tnfa*. (**D**) mRNA levels of *Tgfb* and the SMAD3-target genes *Ctgf* and *Serpine1*. (E) mRNA levels of the macrophage polarization markers *Nos2* and *Arg1*. n = 4–6 per group. Data are presented as the mean ± SEM. Significant differences were established by ANOVA. ***p < 0.001, **p < 0.01, and *p < 0.05 *vs.* control. $^{###}$p < 0.001, $^{##}$p < 0.01, and $^{#}$p < 0.05 *vs.* mice fed the CD-HFD.

reduction in the expression of the M2 marker *Arg1* (Fig. 2D). Collectively, these findings show that PPARβ/δ activation meliorates the metabolic alterations and prevents the liver fibrosis caused by the CD-HFD.

3.2. *Primary HSCs isolated from Ppard$^{-/-}$ mice show increased mRNA levels of Col1a1*

Since HSCs are the central effectors of hepatic fibrosis, we next focused on the role of PPARβ/δ in these cells. In primary HSCs isolated from wild-type (WT) and *Ppard*$^{-/-}$ mice (Fig. 3A), we observed that a deficiency of this nuclear receptor increased the expression levels of *Col1a1* (Fig. 3B), whereas no changes were observed in the expression of *Tgfb* and *Col3a1* (Fig. 3C-D). These findings suggest that, at least in part, *Ppard* deficiency impacts the regulation of a marker of liver fibrosis and HSC activation.

3.3. *PPARβ/δ activation abrogates TGF-β1-mediated cell migration and SMAD3 activation in LX-2 cells*

To evaluate whether the antifibrogenic effects observed in the livers of CD-HFD-fed mice could occur solely through an effect on HSCs, the direct effects of GW501516 were assessed in the human HSC LX-2 cell line, which provides a valuable tool to study liver fibrosis [34]. Since an increase in HSC migration is indicative of cell activation, we examined the effects of GW501516 on cell migration in response to TGF-β1 by conducting wound healing assays in which cell monolayers were serum-starved for 16 hours and then scratched to form cell-free paths. The scratched monolayers were then incubated in media for 24 hours in the presence or absence of TGF-β1 and with or without GW501516. In response to TGF-β1, the cells migrated faster, but GW501516 elicited a robust inhibition of the TGF-β1-triggered closure of the wounds (Fig. 4A). Consistent with this, GW501516 completely abolished the increases in the protein levels of COL1A1 and α-SMA, two reliable markers of HSC activation and liver fibrosis (Fig. 4B). Next, we assessed the activation of SMAD3. This transcription factor is activated via phosphorylation by type I TGF-β receptors and also intracellular kinases such as ERK1/2 [35]. Once phosphorylated, SMAD3 interacts with SMAD4 and translocates to the nucleus, where it binds to the co-activator p300 to activate gene transcription [35]. As expected, TGF-β1 increased SMAD3 phosphorylation, but this was not observed in the LX-2 cells treated with GW501516 (Fig. 4C). Similarly, GW501516 abolished the increase in p300 levels caused by TGF-β1 (Fig. 4D). In accordance with these observations, the livers of *Ppard*$^{-/-}$ mice exhibited increased phosphorylated SMAD3 (Fig. 4E) and p300 protein levels compared to those of WT mice (Fig. 4F), while primary HSCs isolated from *Ppard*$^{-/-}$ mice displayed enhanced *p300* (also named *Ep300*) mRNA levels (Fig. 4G). Overall, these results show that PPARβ/δ activation

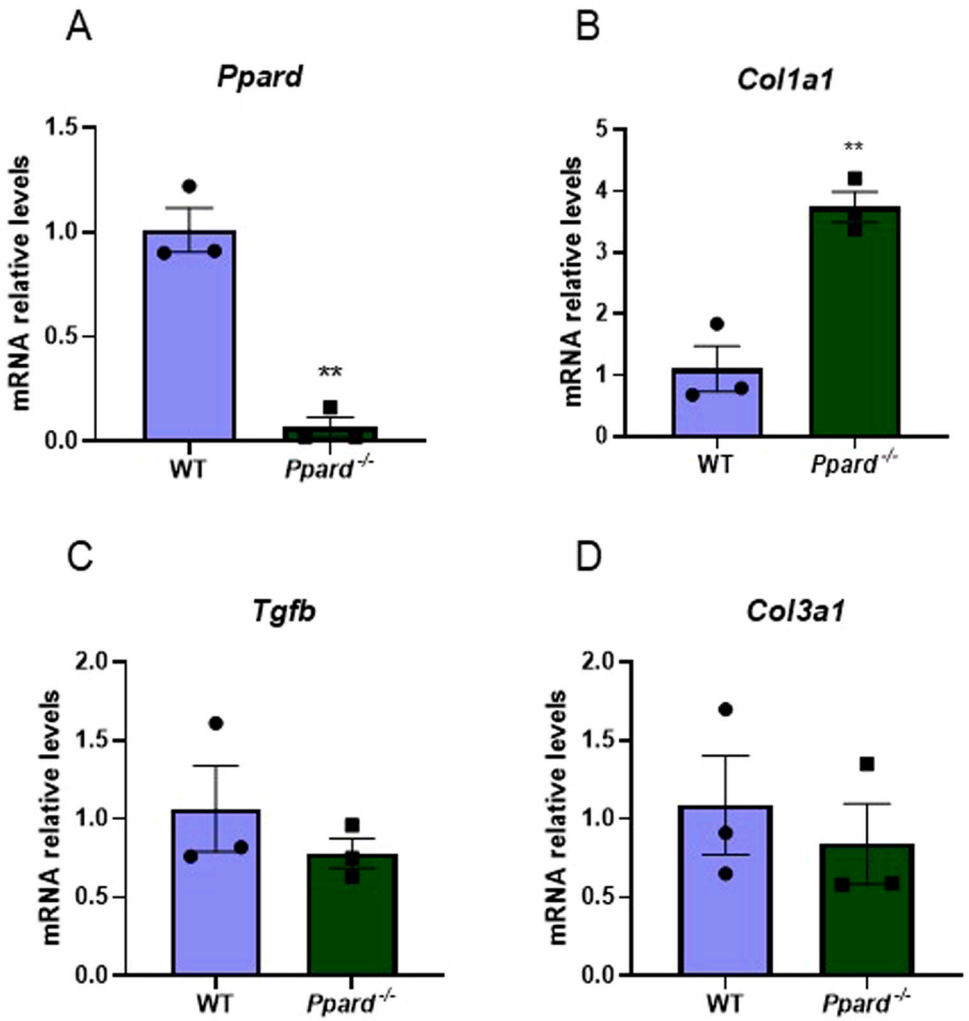

Fig. 3. Primary HSCs isolated from *Ppard*$^{-/-}$ mice show increased mRNA levels of *Col1a1*. mRNA levels of (**A**) *Ppard,* (**B**) *Col1a1*, (**C**) *Tgfb* and (**D**) *Col3a1* in primary HSCs isolated from wild-type (WT) and *Ppard*$^{-/-}$ mice. n = 3 per group. Data are presented as the mean ± SEM. Significant differences were established by Student's t-test. *p < 0.05, **p < 0.01, and ***p < 0.001 *vs.* WT.

abolishes TGF-β1 signaling and also prevents HSC activation, SMAD3 phosphorylation, and increased p300 levels.

3.4. PPARβ/δ activation prevents the reduction in phosphorylated AMPK levels and the increase in phosphorylated ERK1/2 levels caused by TGF-β1 in LX-2 cells

PPARβ/δ agonists activate AMPK [36,37], which reduces hepatic fibrosis in animal models and suppresses the expression of fibrogenic genes in HSCs [35,38,39]. By contrast, TGF-β1 activates ERK1/2, which directly phosphorylates SMAD3, thereby promoting fibrogenesis [12]. Of note, the inhibitory crosstalk between AMPK and ERK1/2 in myotubes [20,21], which so far has not been reported in HSCs to date, might regulate SMAD3 activity and fibrosis. This prompted us to examine the levels of AMPK and ERK1/2 in LX-2 cells exposed to TGF-β1. Treatment with TGF-β1 reduced phosphorylated AMPK levels in HSCs (Fig. 5A). Interestingly, co-incubation of the cells with GW501516 increased AMPK phosphorylation (Fig. 5B) and prevented the increase in phosphorylated ERK1/2 levels caused by TGF-β1 (Fig. 5C). To go deeper into the effects of AMPK activation on HSCs in our conditions, we used the specific AMPK activator A769662. This compound prevented the reduction in phosphorylated AMPK levels caused by TGF-β1 in LX-2 cells (Fig. 6A) and, in parallel, abolished the upregulation of COL1A1 (Fig. 6B) and α-SMA (Fig. 6C). Moreover, A769662 caused a significant reduction in the phosphorylation of SMAD3 (Fig. 6D) and in the increase in p300 levels observed in the cells exposed to TGF-β1 (Fig. 6E). It is worth noting that, in agreement with the presence of an inhibitory crosstalk between AMPK and ERK1/2, the AMPK activator A769662 reduced the levels of phosphorylated ERK1/2 (Fig. 6F). Next, we assessed the effects of ERK1/2 inhibition by using its specific inhibitor U0126. The reduction of ERK1/2 phosphorylation caused by U0126 (Fig. 7A) led to an increase in phosphorylated AMPK levels (Fig. 7B), again supporting the presence of a negative crosstalk between these two kinases in LX-2 cells. Treatment with the ERK1/2 inhibitor also mitigated the increase in COL1A1 (Fig. 7C) and α-SMA (Fig. 7D) levels caused by the exposure to TGF-β1. Similar to that observed with A769662, U0126 also attenuated the increases in phosphorylated SMAD3 (Fig. 7E) and p300 levels (Fig. 7F) caused by TGF-β1. Collectively, these findings suggest that the activation of AMPK prevents the increases in SMAD3 phosphorylation and p300 levels in HSCs by reducing ERK1/2 activation. Therefore, these findings suggest that ERK1/2 inhibition is responsible for the antifibrotic effect of PPARβ/δ and the activation of AMPK.

3.5. PPARβ/δ activation attenuates the increase in phosphorylated ERK1/2 and p300 levels caused by TGF-β1 in LX-2 cells via AMPK

To demonstrate that the effects of ligand-activated PPARβ/δ on HSC

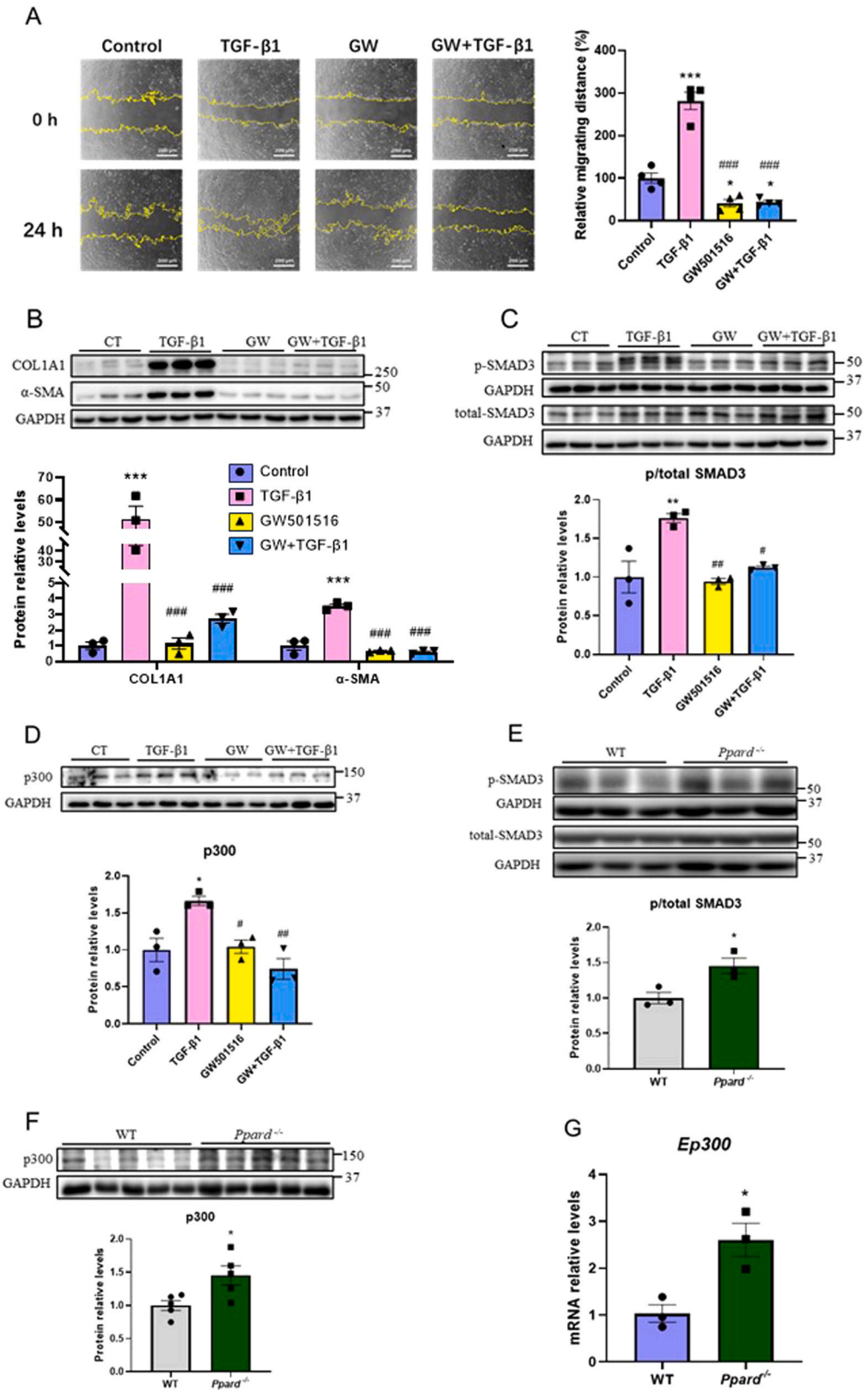

Fig. 4. PPARβ/δ activation abrogates TGF-β1-mediated cell migration and SMAD3 activation in LX-2 cells. (**A**) The wound healing assay was used to detect the ability of PPARβ/δ activation to attenuate TGF-β1-induced migration. The bars on the right present the relative migration distances in percentages. Immunoblot analysis of (**B**) COL1A1 and α-SMA, (**C**) total and phosphorylated SMAD3 and (**D**) p300 in LX-2 cells exposed to 10 ng/ml of TGF-β1 in the presence or absence of 10 μM GW501516 for 24 h. n = 3 per group. Data are presented as the mean ± SEM. Significant differences were established by ANOVA. ***$p < 0.001$, **$p < 0.01$, and *$p < 0.05$ *vs.* control. $^{###}p < 0.001$, $^{##}p < 0.01$, and $^{#}p < 0.05$ *vs.* TGF-β1-incubated cells. Immunoblot analysis of (**E**) total and phosphorylated SMAD3 and (**F**) p300 in the livers of WT and *Ppard*$^{-/-}$ mice. n = 5 per group. (**G**) mRNA levels of *Ep300* in primary HSCs isolated from wild-type (WT) and *Ppard*$^{-/-}$ mice. n = 3 per group. Data are presented as the mean ± SEM. Significant differences were established by Student's t-test. *$p < 0.05$ *vs.* WT.

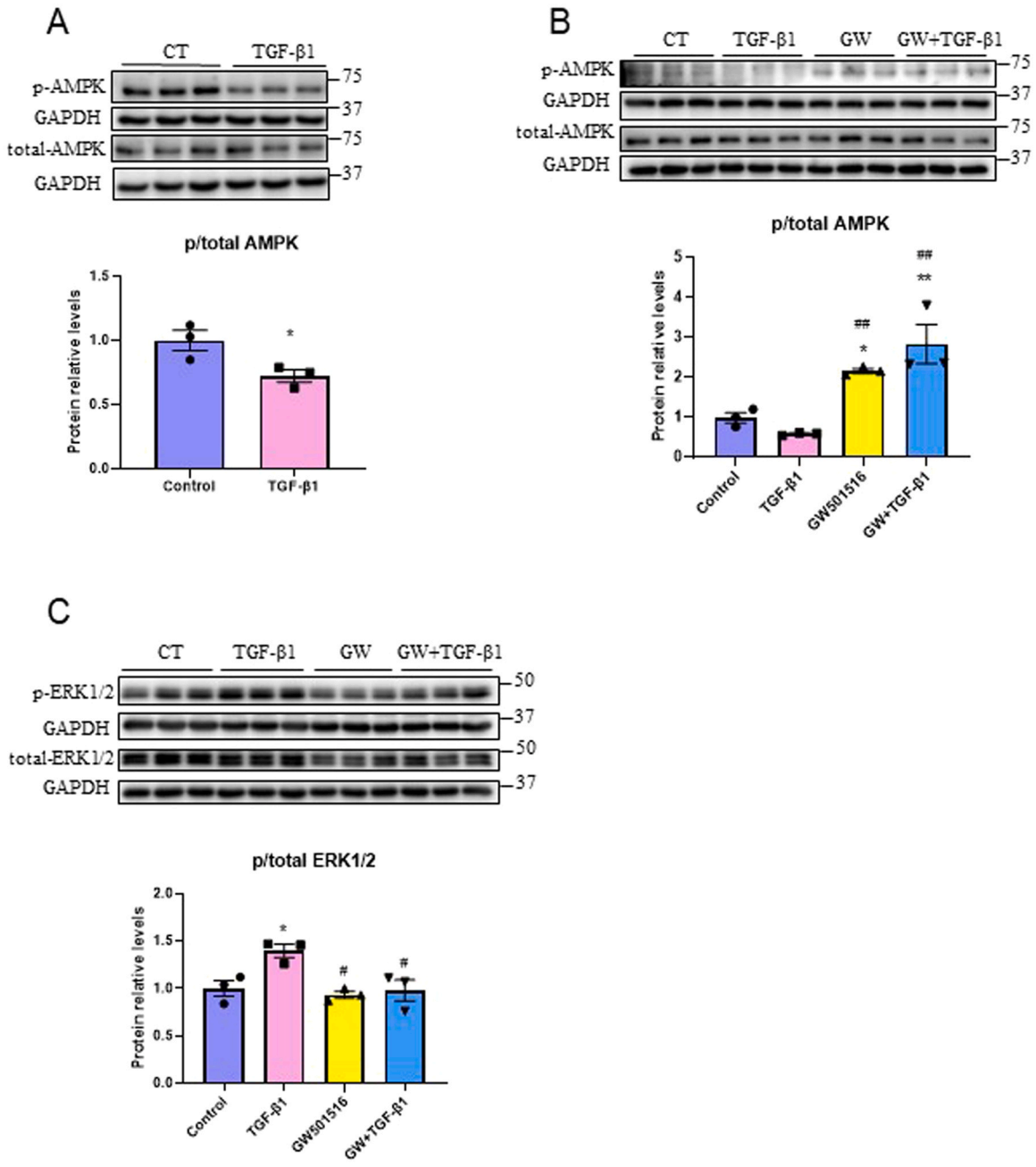

Fig. 5. PPARβ/δ activation prevents the reduction in phosphorylated AMPK levels and the increase in phosphorylated ERK1/2 levels caused by TGF-β1 in LX-2 cells. (**A**) Immunoblot analysis of total and phosphorylated AMPK in LX-2 cells exposed to 10 ng/ml of TGF-β1 for 24 h. n = 3 per group. Data are presented as the mean ± SEM. Significant differences were established by Student's t-test. *$p < 0.05$ *vs.* WT. Immunoblot analysis of (**B**) total and phosphorylated AMPK and (**C**) total and phosphorylated ERK1/2 in LX-2 cells exposed to 10 ng/ml of TGF-β1 in the presence or absence of 10 μM GW501516 for 24 h. n = 3 per group. Data are presented as the mean ± SEM. Significant differences were established by ANOVA. **$p < 0.01$ and *$p < 0.05$ *vs.* control. $^{\#\#}p < 0.01$ and $^{\#}p < 0.05$ *vs.* TGF$^{-\beta}$1-incubated cells.

activation, fibrosis, and p300 levels are mediated by AMPK, we transfected LX-2 cells with control (scrambled) or AMPKα1/2 siRNA. Knockdown of AMPKα1/2 (Supplementary Figure 1) blocked the increase in phosphorylated AMPK levels caused by the PPARβ/δ agonist GW501516 (Fig. 8A). Supporting a role for AMPK in the effects of GW501516 on phosphorylated SMAD3 and ERK1/2 levels and on COL1A1 levels, their increase by TGF-β1 was mitigated by knocking down AMPKα1/2 (Fig. 8A). Likewise, the reduction in p300 levels caused by GW501516 in cells stimulated with TGF-β1 completely disappeared when AMPKα1/2 was knocked down (Fig. 8B). Altogether, these findings confirm that in HSCs stimulated with TGF-β1, PPARβ/δ activation prevents the increase in ERK1/2 phosphorylation, fibrosis, and p300 upregulation via AMPK.

4. Discussion

HSC activation is a central event in the occurrence and progression of liver fibrosis. In response to liver injury, the repair process comprises the activation and transdifferentiation of HSCs into proliferative, migratory, fibrogenic myofibroblast-like cells that cause an excessive accumulation of ECM, subsequent matrix remodeling, and, finally, liver cell dysfunction. Several studies have already unveiled a gene transcription program that deactivates HSCs and involves transcription factors including PPARγ [3,40]. However, the role of PPARβ/δ in hepatic fibrosis remains

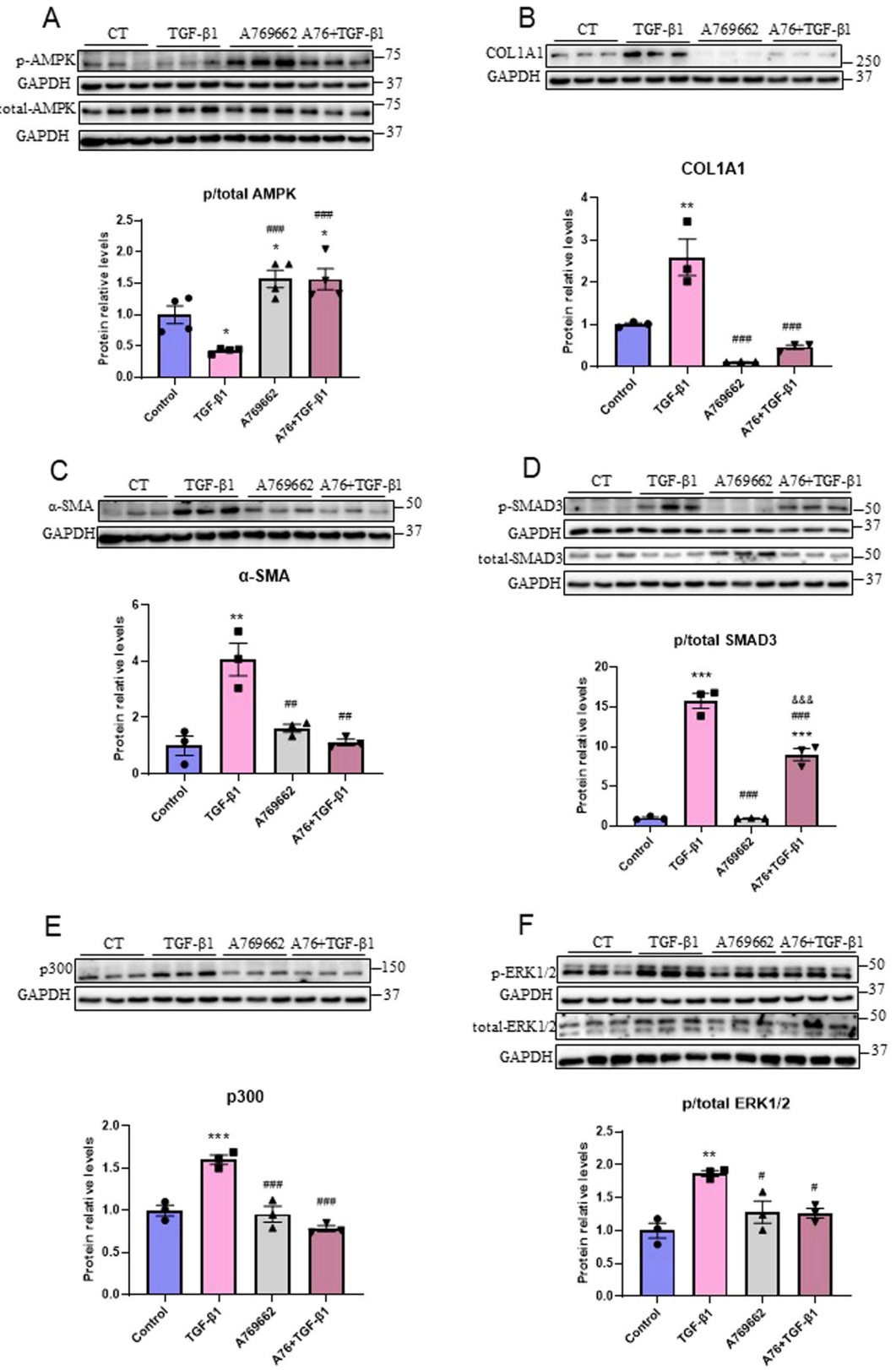

Fig. 6. AMPK activation prevents the increase in fibrosis markers, the phosphorylation of ERK1/2, and the increase in p300 levels caused by TGF-β1 in LX-2 cells. Immunoblot analysis of (**A**) total and phosphorylated AMPK, (**B**) COL1A1, (**C**) α-SMA, (**D**) total and phosphorylated SMAD3, (**E**) p300 and (**F**) total and phosphorylated ERK1/2 in LX-2 cells exposed to 10 ng/ml of TGF-β1 in the presence or absence of 60 μM A769662 for 24 h. n = 3–4 per group. Data are presented as the mean ± SEM. Significant differences were established by ANOVA. ***p < 0.001, **p < 0.01 and *p < 0.05 *vs.* control. $^{###}$p < 0.001, $^{##}$p < 0.01, and $^{#}$p < 0.05 *vs.* TGF-β1-incubated cells.

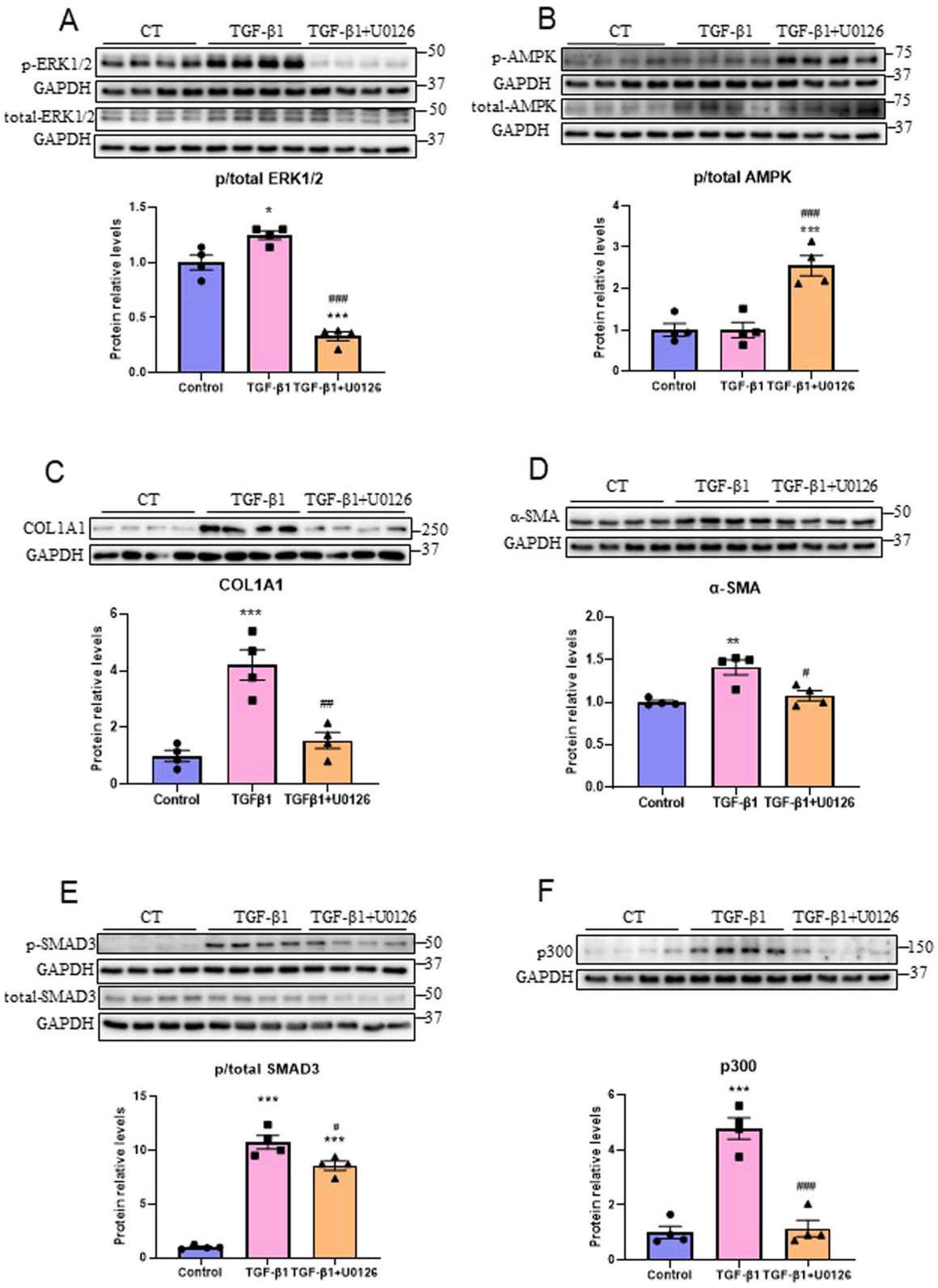

Fig. 7. ERK1/2 inhibition leads to AMPK phosphorylation and prevents the increases in fibrosis markers and p300 levels caused by TGF-β1 in LX-2 cells. Immunoblot analysis of (**A**) total and phosphorylated ERK1/2, (**B**) total and phosphorylated AMPK, (**C**) COL1A1, (**D**) α-SMA, (**E**) total and phosphorylated SMAD3, and (**F**) p300 in LX-2 cells exposed to 10 ng/ml TGF-β1 in the presence or absence of 10 μM U0126 for 24 h. n = 4 per group. Data are presented as the mean ± SEM. Significant differences were established by ANOVA. ***p < 0.001, **p < 0.01 and *p < 0.05 *vs.* control. $^{###}$p < 0.001, $^{##}$p < 0.01, and $^{#}$p < 0.05 *vs.* TGF-β1-incubated cells.

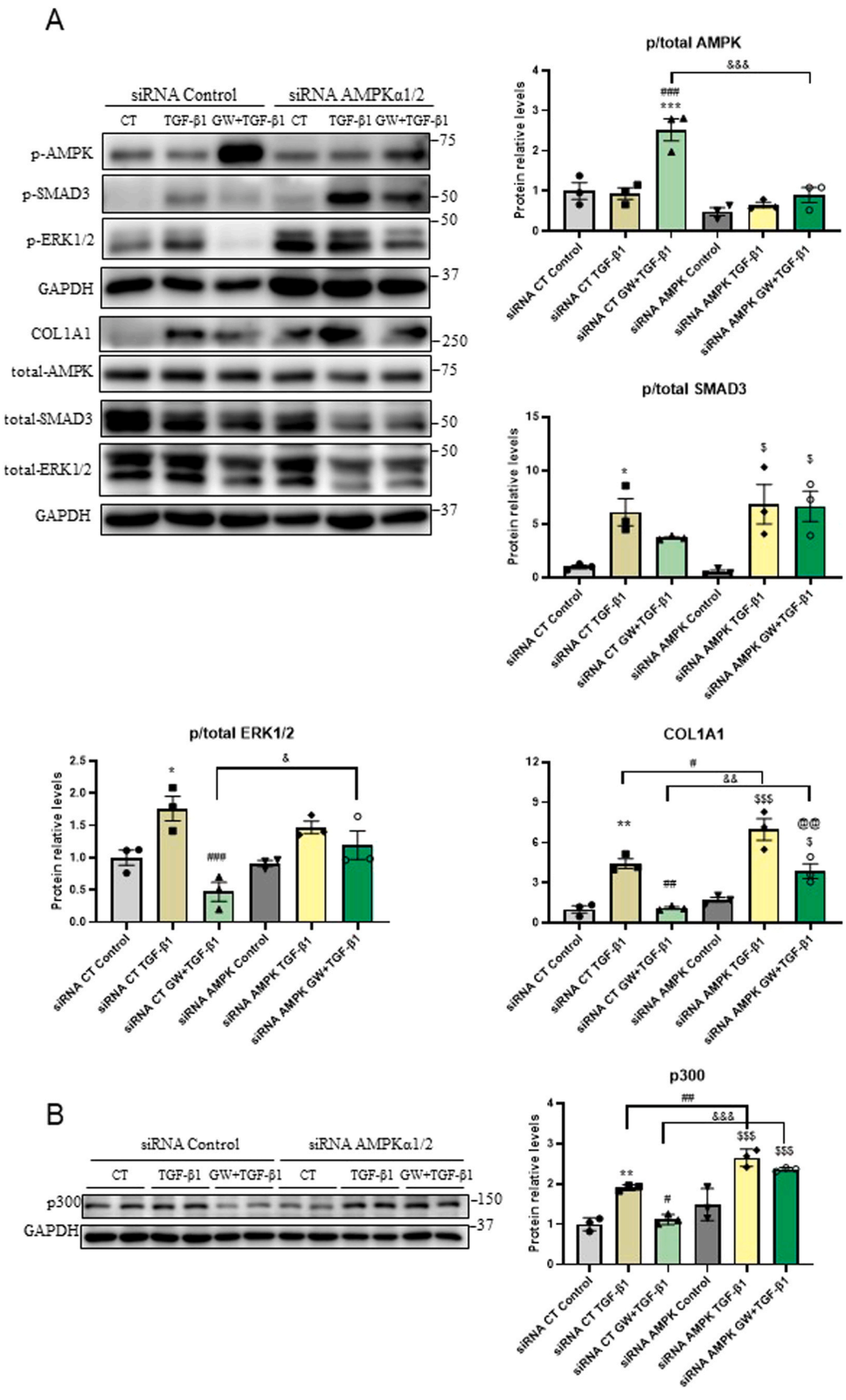

(caption on next page)

Fig. 8. PPARβ/δ activation attenuates the increases in the levels of phosphorylated ERK1/2 and p300 caused by TGF-β1 via AMPK in LX-2 cells. Immunoblot analysis of (**A**) total and phosphorylated AMPK, total and phosphorylated SMAD3, total and phosphorylated ERK1/2, and COL1A1, and (**B**) p300 in LX-2 cells transfected with control (CT) (scrambled) siRNA or AMPKα1/2 siRNA and exposed to 10 ng/ml of TGF-β1 in the presence or absence of 10 μM GW501516 for 24 h. n = 3 per group. Data are presented as the mean ± SEM. Significant differences were established by ANOVA. ***p < 0.001, **p < 0.01, and *p < 0.05 *vs.* CT siRNA. $^{###}$p < 0.001, $^{##}$p < 0.01, and $^{#}$p < 0.05 *vs.* CT siRNA + TGF-β1. $^{&&&}$p < 0.001, $^{&&}$p < 0.01, and $^{&}$p < 0.05 *vs.* CT siRNA + TGF-β1 + GW501516. $^{$$$}$p < 0.001 and $^{$}$p < 0.05 *vs.* AMPK siRNAl. $^{@@}$ p < 0.01 *vs.* AMPK siRNA + TGF-β1.

unclear because of its dual role in promoting [23,24] and repressing [17, 25] these processes. The fibrosis-promoting effect of GW501516 has been previously observed in mice treated chronically with carbon tetrachloride (CCl_4) and may possibly involve the p38 and JNK MAPK pathways in HSCs [23]. The protective effects of PPARβ/δ have been observed with other agonists. The protective effects of GW0742 have not been observed with hepatocytes and HSCs suggesting that paracrine and autocrine events mediated by different cells are involved [25]. Interestingly, the hepatoprotective and antifibrotic effect of HKD3010 is meditated by hepatocytes [17]. In this study, we show that PPARβ/δ activation improves hepatic fibrosis in mice fed a CD-HFD. Consistent with this, we observed that primary HSCs isolated from *Ppard*$^{-/-}$ mice showed increased mRNA levels of *Col1a1*, while PPARβ/δ activation abrogated TGF-β1-mediated cell migration and SMAD3 activation in LX-2 cells. Our findings also point to AMPK activation as the mechanism responsible for the inhibition of TGF-β1-mediated HSC activation and fibrosis by the PPARβ/δ agonist GW501516. In fact, AMPK activation is recognized as a target for treating hepatic fibrosis [41–43]. Several studies have demonstrated that the induction of AMPK activity represses the TGF-β1-induced expression of fibrogenic genes in HSCs [44–46]. AMPK may prevent the activation of HSCs and the development of fibrosis through several mechanisms. For instance, AMPK activation in HSCs attenuates the production of reactive oxygen species (ROS) and HSC activation [47,48], thereby protecting against liver fibrosis. Consistent with this, a recent study reported that the direct AMPK activator PXL770 reduces the activation and proliferation of HSCs [43]. In human HSCs, this AMPK activator suppresses the expression of the key activation marker *ACTA2* (encodes α-SMA) and *COL1A1*, while strongly reducing COL1A1 (also known as procollagen alpha 1) protein secretion. Moreover, it has been reported that AMPK activation disrupts the interaction between SMAD3 and its transcriptional coactivator p300, inducing the proteasomal degradation of p300 to reduce fibrogenic gene expression in HSCs [39]. Additionally, AMPK may inhibit HSC proliferation and promote the apoptosis of these cells via increased nitric oxide production [46]. Here, we report a new mechanism by which PPARβ/δ activation and the subsequent AMPK phosphorylation contribute to the prevention of HSC activation and fibrosis. Our findings indicate that AMPK activation caused by the PPARβ/δ ligand GW501516 inhibits TGF-β1-mediated HSC activation and fibrosis in LX-2 cells by reducing the levels of phosphorylated ERK1/2 (Fig. 9). The potent profibrotic mediator TGF-β1 regulates fibrosis through two pathways: the canonical SMAD-dependent pathway and a non-SMAD signaling pathway [12]. The ERK1/2 signaling pathway forms part of the second non-canonical TGF-β1-dependent pathway and increasing amounts of evidence demonstrate its involvement in fibrosis [12]. Our findings reinforce the role of ERK1/2 in HSC activation and fibrosis since we observed that ERK1/2 inhibition with U0126 attenuated the increases in COL1A1 and α-SMA protein levels as well as the phosphorylation of SMAD3. Interestingly, we [20] and others [21] have demonstrated that an inhibitory crosstalk between AMPK and ERK1/2 exists in mouse myotubes, but it was unknown if this mechanism occurs in human LX-2 cells. Our findings confirm the presence of this inhibitory

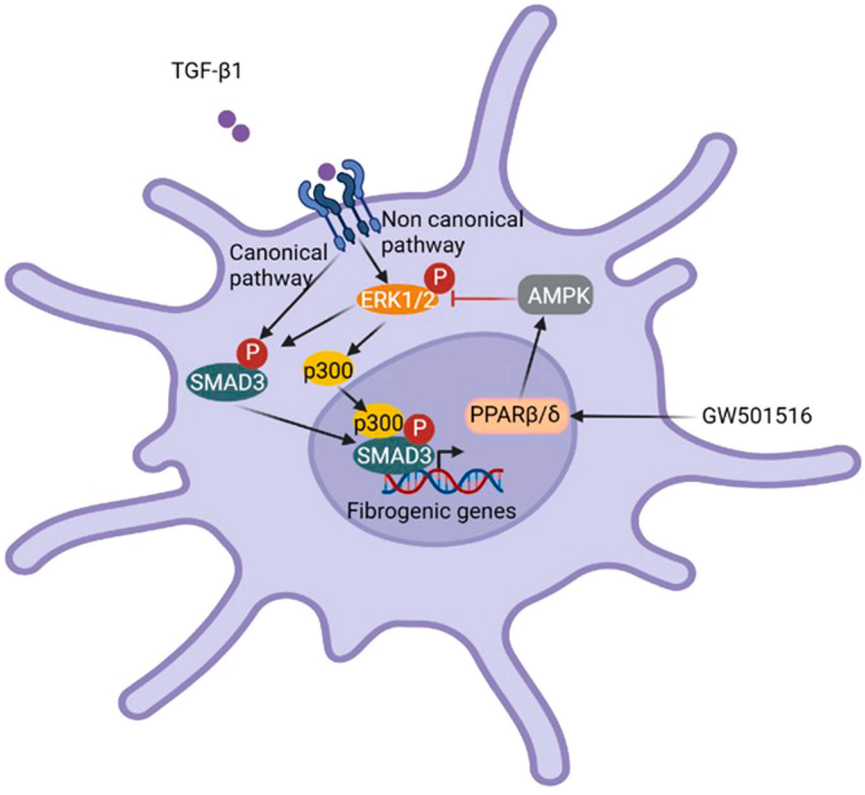

Fig. 9. PPARβ/δ activation prevents HSC activation and fibrosis by promoting AMPK phosphorylation. AMPK inhibits the non-canonical pathway of SMAD3, thereby reducing the activation of SMAD3 and the increase in the levels of the co-activator p300 caused by TGF-β1 in HSCs.

crosstalk in HSCs, providing a new mechanism by which AMPK inhibits HSC activation and fibrosis through the blockade of the ERK1/2 pathway. We propose that the activation of AMPK by a PPARβ/δ agonist inhibits ERK1/2 phosphorylation, thereby attenuating TGF-β1-mediated HSC activation and fibrosis.

Interestingly, it has been reported that TGF-β1 decreases AMPK phosphorylation and increases fibrosis in kidney fibrosis, with AMPK inhibition mimicking or exacerbating the effects of TGF-β1 in renal fibrosis [49]. These findings suggest that TGF-β1 might also induce fibrosis and HSC activation via AMPK downregulation and the subsequent activation of ERK1/2. Along this line, our findings show that HSCs exposed to TGF-β1 present reduced AMPK phosphorylation and increased ERK1/2 phosphorylation. Therefore, this seems to confirm that the modulation of the negative crosstalk between AMPK and ERK1/2 has an impact on HSC activation and fibrosis.

p300 interacts with SMAD3 in a ligand-dependent manner and enhances its transcriptional activity [50]. The findings of this study now provide a role for PPARβ/δ in the regulation of p300 levels via AMPK, as demonstrated by the knockdown of AMPK in LX-2 cells. Accordingly, primary HSCs isolated from *Ppard*$^{-/-}$ mice showed increased mRNA levels of *p300*, indicating that PPARβ/δ controls the expression of p300. In addition, pharmacological inhibition of ERK1/2 increased AMPK phosphorylation and prevented the increase in p300 levels caused by TGF-β1, thereby suggesting that the negative crosstalk between AMPK and ERK1/2 also regulates p300 levels.

Overall, the findings of our study indicate that PPARβ/δ activation reduces hepatic fibrosis by attenuating the TGF-β1-mediated activation of HSCs via the activation of AMPK. This kinase inhibits the phosphorylation of ERK1/2, thereby reducing SMAD3 phosphorylation and HSC activation. In addition, the inhibition of the ERK1/2 pathway by PPARβ/δ and AMPK reduces the levels of the SMAD3 co-activator p300 in LX-2 cells. These data suggest that targeting ERK1/2 might be a therapeutic way of attenuating HSC activation and fibrosis.

In conclusion, our study and those of others reveal that PPARβ/δ uses different pathways in different cell types depending on the agonists and experimental models used to promote or protect against fibrosis. These diverse PPARβ/δ effects call for additional studies to refine the mechanistic characteristics of the responses to this receptor and its synthetic agonists, which will contribute to the evaluation of their potential in treating chronic liver diseases.

Funding

This study was partly supported by the grants PID2021-122116OB-I00 (X.P. and M.V-C.) and PID2021-122766OB-I00 (A.M.V.) funded by MICIU/AEI/10.13039/501100011033 and by "ERDF, A way of making Europe". CIBER de Diabetes y Enfermedades Metabólicas Asociadas (CIBERDEM) is a Carlos III Health Institute project. We also acknowledge support from the CERCA Programme/Generalitat de Catalunya. E. B is a Serra Hunter fellow. Meijian Zhang was supported by a grant from the China Scholarship Council (CSC) (202007565030).

CRediT authorship contribution statement

Lucia Peña: Methodology, Investigation, Formal analysis. **Patricia Rada:** Methodology, Investigation, Formal analysis. **Ángela M Valverde:** Methodology, Investigation, Funding acquisition, Formal analysis. **Walter Wahli:** Writing – review & editing, Investigation. **Xavier Palomer:** Writing – review & editing, Funding acquisition. **Manuel Vazquez-Carrera:** Writing – review & editing, Writing – original draft, Validation, Supervision, Resources, Project administration, Methodology, Investigation, Funding acquisition, Formal analysis, Data curation, Conceptualization. **Meijian Zhang:** Methodology, Investigation, Formal analysis. **Emma Barroso:** Methodology, Investigation, Formal analysis.

Declaration of Competing Interest

None.

Data Availability

Data will be made available on request.

Acknowledgements

We would like to thank the Language Services of the University of Barcelona for revising the manuscript in English.

Appendix A. Supporting information

Supplementary data associated with this article can be found in the online version at doi:10.1016/j.biopha.2024.117303.

References

[1] L. Hammerich, F. Tacke, Hepatic inflammatory responses in liver fibrosis, Nat. Rev. Gastroenterol. Hepatol. 20 (10) (2023) 633–646.
[2] A.C. Sheka, O. Adeyi, J. Thompson, B. Hameed, P.A. Crawford, S. Ikramuddin, Nonalcoholic steatohepatitis: a review, JAMA 323 (12) (2020) 1175–1183.
[3] S. Wang, S.L. Friedman, Found in translation-Fibrosis in metabolic dysfunction-associated steatohepatitis (MASH), Sci. Transl. Med 15 (716) (2023) eadi0759.
[4] I. Mederacke, C.C. Hsu, J.S. Troeger, P. Huebener, X. Mu, D.H. Dapito, J.P. Pradere, R.F. Schwabe, Fate tracing reveals hepatic stellate cells as dominant contributors to liver fibrosis independent of its aetiology, Nat. Commun. 4 (2013) 2823.
[5] T. Kisseleva, D. Brenner, Molecular and cellular mechanisms of liver fibrosis and its regression, Nat. Rev. Gastroenterol. Hepatol. 18 (3) (2021) 151–166.
[6] F. Marra, Hepatic stellate cells and the regulation of liver inflammation, J. Hepatol. 31 (6) (1999) 1120–1130.
[7] R.F. Schwabe, I. Tabas, U.B. Pajvani, Mechanisms of fibrosis development in nonalcoholic steatohepatitis, Gastroenterology 158 (7) (2020) 1913–1928.
[8] B. Dewidar, C. Meyer, S. Dooley, A.N. Meindl-Beinker, TGF-beta in hepatic stellate cell activation and liver fibrogenesis-updated 2019, Cells 8 (2019) 11.
[9] Y. Inagaki, I. Okazaki, Emerging insights into Transforming growth factor beta Smad signal in hepatic fibrogenesis, Gut 56 (2) (2007) 284–292.
[10] K.L. Walton, K.E. Johnson, C.A. Harrison, Targeting TGF-beta mediated SMAD signaling for the prevention of fibrosis, Front Pharm. 8 (2017) 461.
[11] A.K. Ghosh, J. Varga, The transcriptional coactivator and acetyltransferase p300 in fibroblast biology and fibrosis, J. Cell Physiol. 213 (3) (2007) 663–671.
[12] Y.E. Zhang, Non-smad signaling pathways of the TGF-beta family, Cold Spring Harb. Perspect. Biol. 9 (2017) 2.
[13] D.M. El-Tanbouly, W. Wadie, R.H. Sayed, Modulation of TGF-beta/Smad and ERK signaling pathways mediates the anti-fibrotic effect of mirtazapine in mice, Toxicol. Appl. Pharm. 329 (2017) 224–230.
[14] M. Kerroch, D. Guerrot, S. Vandermeersch, S. Placier, L. Mesnard, C. Jouanneau, E. Rondeau, P. Ronco, J.J. Boffa, C. Chatziantoniou, J.C. Dussaule, Genetic inhibition of discoidin domain receptor 1 protects mice against crescentic glomerulonephritis, FASEB J. 26 (10) (2012) 4079–4091.
[15] F.F. Cai, R. Wu, Y.N. Song, A.Z. Xiong, X.L. Chen, M.D. Yang, L. Yang, Y. Hu, M. Y. Sun, S.B. Su, Yinchenhao Decoction Alleviates Liver Fibrosis by Regulating Bile Acid Metabolism and TGF-beta/Smad/ERK Signalling Pathway, Sci. Rep. 8 (1) (2018) 15367.
[16] B. Staels, L. Butruille, S. Francque, Treating NASH by targeting peroxisome proliferator-activated receptors, J. Hepatol. 79 (5) (2023) 1302–1316.
[17] K. Iwaisako, M. Haimerl, Y.H. Paik, K. Taura, Y. Kodama, C. Sirlin, E. Yu, R.T. Yu, M. Downes, R.M. Evans, D.A. Brenner, B. Schnabl, Protection from liver fibrosis by a peroxisome proliferator-activated receptor delta agonist, Proc. Natl. Acad. Sci. USA 109 (21) (2012) E1369–E1376.
[18] S. Francque, G. Szabo, M.F. Abdelmalek, C.D. Byrne, K. Cusi, J.F. Dufour, M. Roden, F. Sacks, F. Tacke, Nonalcoholic steatohepatitis: the role of peroxisome proliferator-activated receptors, Nat. Rev. Gastroenterol. Hepatol. 18 (1) (2021) 24–39.
[19] L.K. Townsend, G.R. Steinberg, AMPK and the endocrine control of metabolism, Endocr. Rev. 44 (5) (2023) 910–933.
[20] L. Salvado, E. Barroso, A.M. Gomez-Foix, X. Palomer, L. Michalik, W. Wahli, M. Vazquez-Carrera, PPARbeta/delta prevents endoplasmic reticulum stress-associated inflammation and insulin resistance in skeletal muscle cells through an AMPK-dependent mechanism, Diabetologia 57 (10) (2014) 2126–2135.
[21] S.L. Hwang, Y.T. Jeong, X. Li, Y.D. Kim, Y. Lu, Y.C. Chang, I.K. Lee, H.W. Chang, Inhibitory cross-talk between the AMPK and ERK pathways mediates endoplasmic reticulum stress-induced insulin resistance in skeletal muscle, Br. J. Pharm. 169 (1) (2013) 69–81.
[22] S. Pu, H. Zhou, Y. Liu, J. Liu, Y. Guo, H. Zhou, Roles of nuclear receptors in hepatic stellate cells, Expert Rev. Gastroenterol. Hepatol. 15 (8) (2021) 879–890.
[23] R. Kostadinova, A. Montagner, E. Gouranton, S. Fleury, H. Guillou, D. Dombrowicz, P. Desreumaux, W. Wahli, GW501516-activated PPARbeta/delta promotes liver

fibrosis via p38-JNK MAPK-induced hepatic stellate cell proliferation, Cell Biosci. 2 (1) (2012) 34.
[24] K. Hellemans, L. Michalik, A. Dittie, A. Knorr, K. Rombouts, J. De Jong, C. Heirman, E. Quartier, F. Schuit, W. Wahli, A. Geerts, Peroxisome proliferator-activated receptor-beta signaling contributes to enhanced proliferation of hepatic stellate cells, Gastroenterology 124 (1) (2003) 184–201.
[25] W. Shan, P.S. Palkar, I.A. Murray, E.I. McDevitt, M.J. Kennett, B.H. Kang, H. C. Isom, G.H. Perdew, F.J. Gonzalez, J.M. Peters, Ligand activation of peroxisome proliferator-activated receptor beta/delta (PPARbeta/delta) attenuates carbon tetrachloride hepatotoxicity by downregulating proinflammatory gene expression, Toxicol. Sci. 105 (2) (2008) 418–428.
[26] M.J. Zarzuelo, M. Gomez-Guzman, R. Jimenez, A.M. Quintela, M. Romero, M. Sanchez, A. Zarzuelo, J. Tamargo, F. Perez-Vizcaino, J. Duarte, Effects of peroxisome proliferator-activated receptor-beta activation in endothelin-dependent hypertension, Cardiovasc Res 99 (4) (2013) 622–631.
[27] A. Villar-Lorenzo, P. Rada, E. Rey, P. Maranon, A.I. Arroba, B. Santamaria, J. Saiz, F.J. Ruperez, C. Barbas, C. Garcia-Monzon, A.M. Valverde, A. Gonzalez-Rodriguez, Insulin receptor substrate 2 (IRS2) deficiency delays liver fibrosis associated with cholestatic injury, Dis. Model Mech. 12 (2019) 7.
[28] S.L. Friedman, F.J. Roll, Isolation and culture of hepatic lipocytes, Kupffer cells, and sinusoidal endothelial cells by density gradient centrifugation with Stractan, Anal. Biochem 161 (1) (1987) 207–218.
[29] R.A. Rippe, G. Almounajed, D.A. Brenner, Sp1 binding activity increases in activated Ito cells, Hepatology 22 (1) (1995) 241–251.
[30] J.C. McGrath, E. Lilley, Implementing guidelines on reporting research using animals (ARRIVE etc.): new requirements for publication in BJP, Br. J. Pharm. 172 (13) (2015) 3189–3193.
[31] T. Tanaka, J. Yamamoto, S. Iwasaki, H. Asaba, H. Hamura, Y. Ikeda, M. Watanabe, K. Magoori, R.X. Ioka, K. Tachibana, Y. Watanabe, Y. Uchiyama, K. Sumi, H. Iguchi, S. Ito, T. Doi, T. Hamakubo, M. Naito, J. Auwerx, M. Yanagisawa, T. Kodama, J. Sakai, Activation of peroxisome proliferator-activated receptor delta induces fatty acid beta-oxidation in skeletal muscle and attenuates metabolic syndrome, Proc. Natl. Acad. Sci. USA 100 (26) (2003) 15924–15929.
[32] W. Zhang, R. Lang, Macrophage metabolism in nonalcoholic fatty liver disease, Front Immunol. 14 (2023) 1257596.
[33] K. Kang, S.M. Reilly, V. Karabacak, M.R. Gangl, K. Fitzgerald, B. Hatano, C.H. Lee, Adipocyte-derived Th2 cytokines and myeloid PPARdelta regulate macrophage polarization and insulin sensitivity, Cell Metab. 7 (6) (2008) 485–495.
[34] L. Xu, A.Y. Hui, E. Albanis, M.J. Arthur, S.M. O'Byrne, W.S. Blaner, P. Mukherjee, S.L. Friedman, F.J. Eng, Human hepatic stellate cell lines, LX-1 and LX-2: new tools for analysis of hepatic fibrosis, Gut 54 (1) (2005) 142–151.
[35] X.C. Dong, K. Chowdhury, M. Huang, H.G. Kim, Signal transduction and molecular regulation in fatty liver disease, Antioxid. Redox Signal 35 (9) (2021) 689–717.
[36] M. Zarei, D. Aguilar-Recarte, X. Palomer, M. Vazquez-Carrera, Revealing the role of peroxisome proliferator-activated receptor beta/delta in nonalcoholic fatty liver disease, Metabolism 114 (2021) 154342.
[37] M. Vazquez-Carrera, Unraveling the Effects of PPARbeta/delta on Insulin Resistance and Cardiovascular Disease, Trends Endocrinol. Metab. 27 (5) (2016) 319–334.
[38] P. Zhao, X. Sun, C. Chaggan, Z. Liao, K. In Wong, F. He, S. Singh, R. Loomba, M. Karin, J.L. Witztum, A.R. Saltiel, An AMPK-caspase-6 axis controls liver damage in nonalcoholic steatohepatitis, Science 367 (6478) (2020) 652–660.
[39] J.Y. Lim, M.A. Oh, W.H. Kim, H.Y. Sohn, S.I. Park, AMP-activated protein kinase inhibits TGF-beta-induced fibrogenic responses of hepatic stellate cells by targeting transcriptional coactivator p300, J. Cell Physiol. 227 (3) (2012) 1081–1089.
[40] X. Li, Y. Chen, S. Wu, J. He, L. Lou, W. Ye, J. Wang, microRNA-34a and microRNA-34c promote the activation of human hepatic stellate cells by targeting peroxisome proliferator-activated receptor gamma, Mol. Med Rep. 11 (2) (2015) 1017–1024.
[41] Z. Liang, T. Li, S. Jiang, J. Xu, W. Di, Z. Yang, W. Hu, Y. Yang, AMPK: a novel target for treating hepatic fibrosis, Oncotarget 8 (37) (2017) 62780–62792.
[42] P. Zhao, A.R. Saltiel, From overnutrition to liver injury: AMP-activated protein kinase in nonalcoholic fatty liver diseases, J. Biol. Chem. 295 (34) (2020) 12279–12289.
[43] P. Gluais-Dagorn, M. Foretz, G.R. Steinberg, B. Batchuluun, A. Zawistowska-Deniziak, J.M. Lambooij, B. Guigas, D. Carling, P.A. Monternier, D.E. Moller, S. Bolze, S. Hallakou-Bozec, Direct AMPK activation corrects NASH in rodents through metabolic effects and direct action on inflammation and fibrogenesis, Hepatol. Commun. 6 (1) (2022) 101–119.
[44] P. Kumar, T. Smith, K. Rahman, N.E. Thorn, F.A. Anania, Adiponectin agonist ADP355 attenuates CCl4-induced liver fibrosis in mice, PLoS One 9 (10) (2014) e110405.
[45] X. Zhai, H. Qiao, W. Guan, Z. Li, Y. Cheng, X. Jia, Y. Zhou, Curcumin regulates peroxisome proliferator-activated receptor-gamma coactivator-1alpha expression by AMPK pathway in hepatic stellate cells in vitro, Eur. J. Pharm. 746 (2015) 56–62.
[46] Z. Dong, L. Su, S. Esmaili, T.J. Iseli, M. Ramezani-Moghadam, L. Hu, A. Xu, J. George, J. Wang, Adiponectin attenuates liver fibrosis by inducing nitric oxide production of hepatic stellate cells, J. Mol. Med (Berl.) 93 (12) (2015) 1327–1339.
[47] Y. Yang, Z. Zhao, Y. Liu, X. Kang, H. Zhang, M. Meng, Suppression of oxidative stress and improvement of liver functions in mice by ursolic acid via LKB1-AMP-activated protein kinase signaling, J. Gastroenterol. Hepatol. 30 (3) (2015) 609–618.
[48] A. Caligiuri, C. Bertolani, C.T. Guerra, S. Aleffi, S. Galastri, M. Trappoliere, F. Vizzutti, S. Gelmini, G. Laffi, M. Pinzani, F. Marra, Adenosine monophosphate-activated protein kinase modulates the activated phenotype of hepatic stellate cells, Hepatology 47 (2) (2008) 668–676.
[49] S. Thakur, S. Viswanadhapalli, J.B. Kopp, Q. Shi, J.L. Barnes, K. Block, Y. Gorin, H. E. Abboud, Activation of AMP-activated protein kinase prevents TGF-beta1-induced epithelial-mesenchymal transition and myofibroblast activation, Am. J. Pathol. 185 (8) (2015) 2168–2180.
[50] A. Nishihara, J.I. Hanai, N. Okamoto, J. Yanagisawa, S. Kato, K. Miyazono, M. Kawabata, Role of p300, a transcriptional coactivator, in signalling of TGF-beta, Genes Cells 3 (9) (1998) 613–623.